Iranian Journal of Geophysics, Vol 15 No 4, 2022, Page 37– 52 (Research Article)
DOI: 10.30499/IJG.2021.253584.1297

A Comparison of impedance invariants and GB decomposition method for magnetotelluric data analysis; A Case study from SW Iran

Mansoure Montahaei[1*] and Sakineh Najafi[2]

[1]*Assistant Professor, Institute of Geophysics, University of Tehran, Tehran, Iran*
[2]*M.Sc student, Institute of Geophysics, University of Tehran, Tehran, Iran*

(Received: 30October 2020, Accepted: 16 May 2021)

Abstract

Dimensionality and distortion analysis of the measured magnetotelluric (MT) data are challenging procedures to conclude the main properties of regional geo-electric structure (e.g., its strike direction) and quantify the influence of superficial distorting bodies. In this paper, we applied several analysis methods to the same data set from southwest Zagros to determine the dimensionality and degree of the inherent distortion in the data and to recover the regional responses. Results show that the regional 2D responses can be better retrieved in a two-step procedure: First, the dimensionality and distortion are classified by impedance invariants and then, the Groom-Baily (GB) method is applied to remove distortion effects and to estimate the regional strike and principal impedances.

An audio-magnetotelluric (AMT) data set acquired at 19 stations along a profile in the southwest of Simply Folded Belt (SFB) of the Zagros Mountains is investigated. The Bahr and WAL invariants confirm regional 1D and 2D structures with local galvanic distortion at most periods. The GB decomposition of MT impedance data reveals period-independent distortion parameters. The strike analysis on all data whose principal phase differences are greater than 5˚ shows a regional trend of about 30˚. 2D inductive effects were also retrieved by removing distortion effects from the measured data.

Keywords: Audio-magnetotelluric, dimensionality, distortion, strike, Zagros

[*] Corresponding author: mmontaha@ut.ac.ir

1 Introduction

Audio magnetotelluric (AMT) method is widely used for hydro-geological studies (Brasse and Rath, 1997; Giroux et al., 1997; Tarabees et al., 2017) due to its suitable exploration depth (0.2-2 km) which is large enough to penetrate conductive surficial sedimentary layers with the ability to discriminate between brine and fresh water bearing layers. The impedance tensor elements ($\mathbf{Z}_{ij}(\omega)$) are the MT transfer functions calculated from the perpendicular components of the time-varying electric field ($\mathbf{E}_i(\omega)$) and magnetic field intensity ($\mathbf{H}_j(\omega)$) measured at the earth's surface:

$$\mathbf{Z_{ij}} = \frac{\mathbf{E_i}}{\mathbf{H_j}} (\mathbf{i}, \mathbf{j} = \mathbf{x}, \mathbf{y}) \quad (1)$$

Alternatively, the elements of magnetotelluric tensor (MT tensor), $\mathbf{M}_{ij}(\omega)$, are defined as the ratio of perpendicular components of the electric and magneticfields ($\mathbf{B}_j(\omega)$):

$$\mathbf{M_{ij}} = \frac{\mathbf{E_i}}{\mathbf{B_j}} (\mathbf{i}, \mathbf{j} = \mathbf{x}, \mathbf{y}) \quad (2)$$

The real-earth electrical structure is very complex, and the scales of the conducting elements vary significantly in nature. Moreover, diffusive EM fields, employed in MT exploration, have restrictions in resolution and sensitivity and cannot model the earth at the full scale. One needs to estimate the actual subsurface structures with more simple structures by studying the dominant dimensionality of the target area (Mahallati and Montahaei, 2019). Dimensionality analysis of the MT tensor data determines whether subsurface resistivity structure could be estimated as 1D (or horizontally layered), 2D with invariant resistivity along regional strike, or 3D. Furthermore, shallow small-scale lateral inhomogeneities severely distort measured electric field components and cause unreliable imaging of the subsurface electrical resistivity (Chave and Jones, 2012).

Several methods have been developed to overcome the above mentioned problems. Some authors assumed that the regional conductivity structure is 1D or 2D, leading to a particular form of the impedance responses. Zhang et al. (1987) adopted a 2D/2D galvanic distortion model for local/regional composite electrical model of the underlying structure. Groom and Bailey (1991) and Mc-Nice and Jones (2001) supposed a 3D/2D distortion model that allowed the retrieval of a strike of regional structure as well as distortion parameters characterizing the effects of local 3D inhomogenities. Cerv et al. (2010) applied multi-site, multi-frequency GB decomposition and determined the range of acceptable parameters employing Bayesian statistics. Alternatively, the phase tensor method (Caldwell et al. 2004) and the WAL invariants (Weaver et al. 2000) make no assumption about the regional conductivity structure.

In this study, the results of GB decomposition and the WAL invariants for dimensionality and distortion analysis of the MT data were compared. Considering the limitations of these methods, we show they may fail in some particular dimensionality cases, and when individually applied, they could not extract adequate information from measured data. We suggest a combined approach comprising subsequent use of the WAL invariants and the GB method. In this strategy, first, the analysis starts with the WAL invariants so that the dimensionality and distortion effects at different period bands are classified for each site. Next, for proper period bands that show a clear sign of 3D/2D distortion model, the analysis is switched to the GB decomposition method to remove distortion effects and retrieve regional impedances. We compared the results of the proposed approach for two theoretical models and a field dataset from the southwest of the simply folded belt (SFB) in the Zagros Mountains.

2 Dimensionality and Distortion Analysis of Magnetotelluric Data

2-1 Impedance invariants and MT data analysis

Rotational invariants of the impedance or MT tensors are parameters derived analytically from the tensor elements, and are free from the rotation of the horizontal axis on the earth's surface.

2-1-1 Bahr rotational invariants

Bahr (1991) proposed four rotational invariants (κ, μ, η, Σ) of impedance tensor (equation (1)), two distortion angles (β_x, β_y), and their corresponding thresholds for model classification. The description of these parameters, their threshold values, and the model classes are summarized in Table 1. μ measures the phase difference of impedance tensor elements and is the 1D indicator. η measures the phase difference of the column-wise elements of the impedance tensor and is the phase sensitive skewness. μ and η determine whether the impedance tensor can be described by the superimposition models (3D/1D and 3D/2D models, respectively).

Table 1. Illustrative parameters suggested by Bahr (1991) for distortion classification.

	κ	μ	Σ	η	β_x	β_y
Threshold	0.1	0.05	0.05	0.3	min=5° max=20°	min=5° max=20°
1) 1D	$<\tau_\kappa$	$<\tau_\mu$	$<\tau_\Sigma$	$<\tau_\eta$	-	-
1) 2D	$<\tau_\kappa$	$<\tau_\mu$	$>\tau_\Sigma$	$<\tau_\eta$	-	-
3) 3D/2D Weak local distortion	$>\tau_\kappa$	$>\tau_\mu$	$>\tau_\Sigma$	$<\tau_\eta$	<min <max	<max <min
4) 3D/2D 2D anomaly in twisted coordinate	$>\tau_\kappa$	$>\tau_\mu$	$>\tau_\Sigma$	$<\tau_\eta$	$=\beta_y$	$=\beta_x$
5) 3D/2D strong local distortion	$>\tau_\kappa$	$>\tau_\mu$	$>\tau_\Sigma$	$<\tau_\eta$	>min >max	>max >min
6) 3D/2D strong local current chanelling	$>\tau_\kappa$	$>\tau_\mu$	$>\tau_\Sigma$	$<\tau_\eta$	=90- β_y	=90- β_x
7) 3D	$>\tau_\kappa$	$>\tau_\mu$	$>\tau_\Sigma$	$>\tau_\eta$	-	-

Equations $S_1=Z_{xx}+Z_{yy}$, $S_2=Z_{xy}+Z_{yx}$, $D_1=Z_{xx}-Z_{yy}$, $D_2=Z_{xy}-Z_{yx}$

$$\eta=\frac{\sqrt{[\mathbf{D}_1,\mathbf{S}_2]-[\mathbf{S}_1,\mathbf{D}_2]}}{|\mathrm{D}_2|},\mu=\frac{\sqrt{[D_1,S_2]+[S_1,D_2]}}{|D_2|}$$

$$[\mathbf{C}_1,\mathbf{C}_2]=\mathrm{Im}(\mathbf{C}_2\mathbf{C}_1^*)=\mathrm{Re}\mathbf{C}_1\mathrm{Im}\mathbf{C}_2-\mathrm{Re}\mathbf{C}_2\,\mathrm{Im}\mathbf{C}_1$$

$$\Sigma=\frac{D_1^2+S_2^2}{D_2^2}$$

$$\kappa=\frac{|S_1|}{|D_2|}$$

2-1-2 WAL rotational invariants and WALDIM code

Weaver et al., (2000) introduced seven independent (I_1, I_2, … , I_7) and one (Q) dependent rotational invariants of the MT tensor (equation (2)), termed WAL invariants. Table 2 summarizes the description of WAL invariants and the seven classes of MT tensor. Invariants I_1 and I_2 provide information about the resistivity and phase of a regional 1D structure. The annulment of other invariants determines whether the subsurface electrical structure is purely 2D (class2), 2D contaminated by different galvanic distortions (classes 3-6) or 3D (class 7). However, WAL invariants calculated from noisy MT measurements are practically non-zero and it is essential to introduce threshold values beneath which we could assume the invariants are zero.

A FORTRAN code termed WALDIM (Marti et al. 2009) calculates WAL rotational invariants of the MT tensors considering data errors to provide a robust description of the dimensionality and galvanic distortion parameters. Marti et al. (2010) extended the WAL dimensionality criteria to include extra conditions discriminating isotropic and anisotropic media responses in dimensionality analysis. They investigated several synthetic anisotropic models and showed that the main signature of anisotropy occurs in

2D situations, where invariant parameters recommend a regional 2D structure but the strikes obtained from the real and imaginary parts of the tensor **M** are not consistent and do not agree with $\theta_{3D/2D}$ (the strike of 3D/2D superposition model).

Table 2. Illustrative parameters suggested by Weaver et al. (2000) for distortion classification.

Dimensionality Class	I_1	I_2	I_3	I_4	I_5	I_6	I_7	Q
1) 1-D	$>\tau_I$	$>\tau_I$	$<\tau_I$	$<\tau_I$	$<\tau_I$	$<\tau_I$	undefined	$<\tau_Q$
2) 2-D	$>\tau_I$	$>\tau_I$	$>\tau_I$	$>\tau_I$	$<\tau_I$	$<\tau_I$	$<\tau_I$	$>\tau_Q$
3) 3D/1D 2D diag Galvanic distortion over a 1D or 2D structure resulting in a diagonal MT tensor	$>\tau_I$	$>\tau_I$	$>\tau_I$	$>\tau_I$	$<\tau_I$	$<\tau_I$	undefined	$<\tau_Q$
4) 3D/1D 2D Galvanic distortion over a 1D or 2D structure (non-recoverable strike direction)	$>\tau_I$	$>\tau_I$	$>\tau_I$	$>\tau_I$	$>\tau_I$	$<\tau_I$	undefined	$<\tau_Q$
5) 3D/2D twist Galvanic distortion (only twist) over a 2D regional structure	$>\tau_I$	$>\tau_I$	$>\tau_I$	$>\tau_I$	$>\tau_I$	$<\tau_I$	$<\tau_I$	$>\tau_Q$
6) 3D/2D General case of galvanic distortion over a 2D structure	$>\tau_I$	$>\tau_I$	$>\tau_I$	$>\tau_I$	$>\tau_I$	$>\tau_I$	$<\tau_I$	$>\tau_Q$
7) 3D	$>\tau_I$	$>\tau_I$	$>\tau_I$	$>\tau_I$	$>\tau_I$	$>\tau_I$	$>\tau_I$	$>\tau_Q$
Equations $\Lambda_1=M_{xx}+M_{yy}=\lambda_1+i\eta_1$ $\Lambda_2=M_{xy}+M_{yx}=\lambda_2+i\eta_2$ $\Lambda_3=M_{xx}-M_{yy}=\lambda_3+i\eta_3$ $\Lambda_4=M_{xy}-M_{yx}=\lambda_4+i\eta_4$	$d_{ij}=\frac{\lambda_i\eta_j-\lambda_j\eta_i}{I_1I_2}$		$I_1=\sqrt{\lambda_1^2+\lambda_4^2}$	$I_2=\sqrt{\eta_1^2+\eta_4^2}$	$I_3=\frac{\sqrt{\lambda_2^2+\lambda_3^2}}{I_1}$	$I_4=\frac{\sqrt{\eta_2^2+\eta_3^2}}{I_2}$	$I_5=S_{41}$ $I_6=d_{41}$	$Q=\sqrt{(d_{12}-d_{34})^2+(d_{13}+d_{24})^2}$ $I_7=\frac{d_{41}-d_{23}}{Q}$
	$S_{ij}=\frac{\lambda_i\eta_j+\lambda_j\eta_i}{I_1I_2}$							

2-2 GB Tensor Decomposition

Groom and Bailey (1991) presumed a 3D/2D distortion model for local/regional structures. They separated galvanic effects into determinable and indeterminable parts and characterized the determinable part in terms of the rotation (twist, $tg^{-1}t$) and shear ($tg^{-1}e$) of the regional telluric currents. Under the GB decomposition approach, the measured impedance tensor can be written as a seven-parameter model descriptive of geoelectric strike (θ), the 2D regional impedances (Z_{xy}, Z_{yx}) and the two descriptors of telluric distortion (t, e):

$$Z_{measured} = RTSZ_{2D}R^T \quad (3)$$

$$Z_{2D}=\begin{bmatrix}0 & Z_{xy}\\ -Z_{yx} & 0\end{bmatrix}, R=\begin{bmatrix}cos\theta & -sin\theta\\ sin\theta & cos\theta\end{bmatrix}$$

$$TS=\begin{bmatrix}1-te & e-t\\ e+t & 1+te\end{bmatrix}$$

Groom and Bailey (1991) used a least square method to fit the decomposition model (equation (3)) with measured data, site-by-site and frequency-by-frequency. The calculation of confidence limits for the derived parameters was performed using a bootstrap approach.

2-3 Theoretical models

In order to compare the application of the above mentioned methods, two synthetic examples are presented. The first is from an electrically anisotropic earth situation used by Heise and Pous (2001) to investigate the anisotropy imprints in MT measurements. The second example is a 2D earth background used by Ledo (2006) for synthetic studies.

2-3-1 Synthetic example 1

The first model (Fig. 1a) comprises a fault between two media of 20 and 2000 Ωm, underlain by an anisotropic layer with principal resistivities 20/1000 Ωm and an anisotropy strike direction of α_s=30˚. A conductive surficial layer (thickness = 260 m, resistivity = 20 Ωm) and a resistive thick layer (thickness = 10 km, resistivity = 5000 Ωm) cover the model. The synthetic MT data were calculated using the finite difference algorithm of Pek and Verner (1997).

An unconstrained GB decomposition method was applied to analyze synthetic dataset. The overall RMS misfit of the distortion model to the data and the recovered distortion parameters (shear and twist angles) are presented as histograms in Fig. 2. The results show that the 3D/2D galvanic distortion model inherent in GB method fit the data well within an acceptable RMS of below 1.5 at almost all sites and periods. Furthermore, the recovered distortion parameters are not negligible. This example shows that the GB method could not recognize electrical anisotropy signature in MT data. The method recovers distortion parameters, representative of local 3D inhomogeneities, which are not visible in the original model. Accordingly, the recovered shear and twist angles are artifacts of distortion analysis applied to the anisotropic MT responses.

In the next step, WAL rotational invariants were applied for dimensionality and distortion analysis of the synthetic data. The obtained dimensionality pattern (Fig. 3) shows clear indication of the electrical anisotropy in MT responses. In all 3D/2D cases, invariant values show two-dimensionality, but strike directions recovered from the real and imaginary MT tensors are different. As a result, the GB decomposition approach is not appropriate for distortion analysis of the synthetic dataset.

2-3-2 Synthetic example 2

As the second synthetic example, a contact between conductive and resistive blocks covered by a 2-km thick layer of 100 Ωm resistivity (Fig. 1b) was considered. A conductive body of 10 Ωm resistivity is embedded in the center of the model. The finite difference algorithm of Rodi and Mackie (2001) was used to generate forward model responses. The regional 2D impedances calculated at 11 stations were distorted by multiplication with different synthetic matrices of galvanic distortion. Gaussian scatter with the magnitude of 5% of the impedance element, resembling experimental noise, was added to the distorted data. WAL dimensionality analysis was performed using the threshold values of τ_I=0.15 and τ_Q=0.1. The results (Fig. 4) coincide well with the original model of the regional geo-electric structure; they rule out regional 3D structure and show distortion imprints at all stations and frequencies.

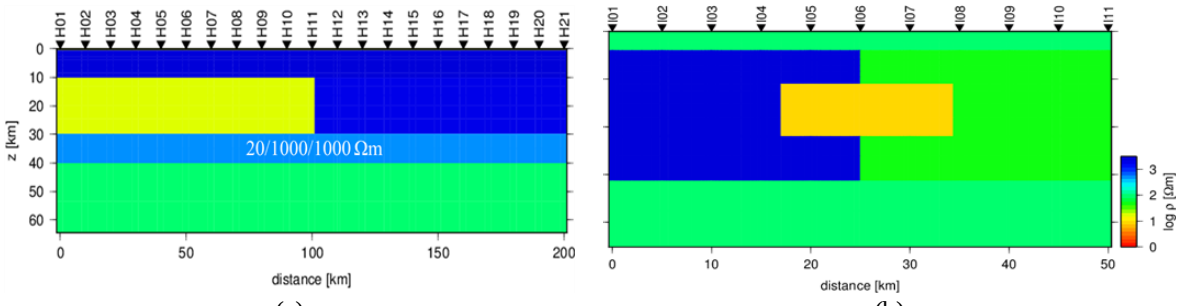

(a) (b)

Fig1. Cross-section of models 1a (left) and 1b (right) used as synthetic examples.

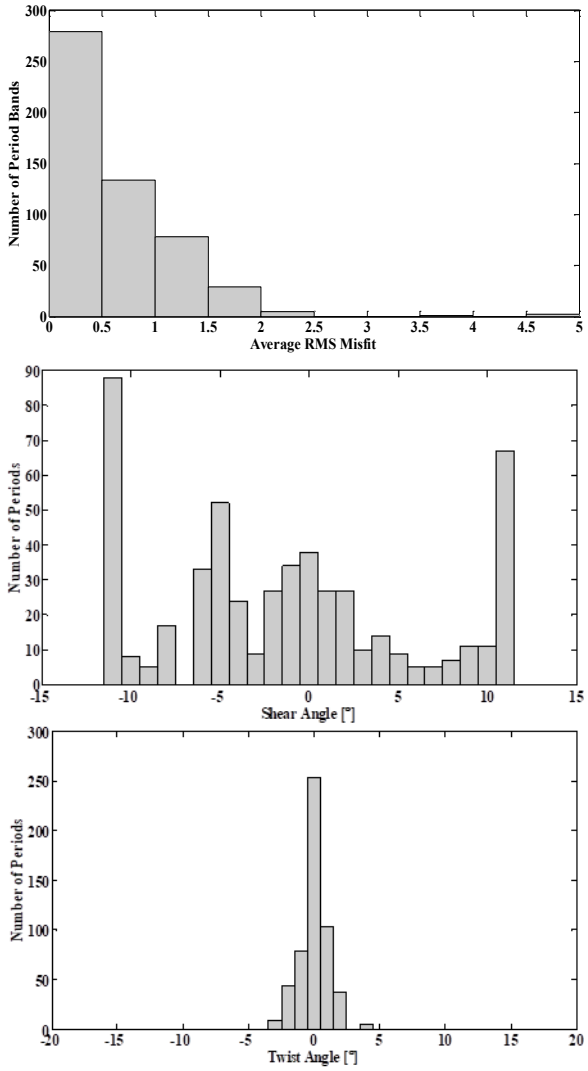

Fig 2. Distribution of the twist and shear angles and the average RMS misfits for synthetic dataset example 1.

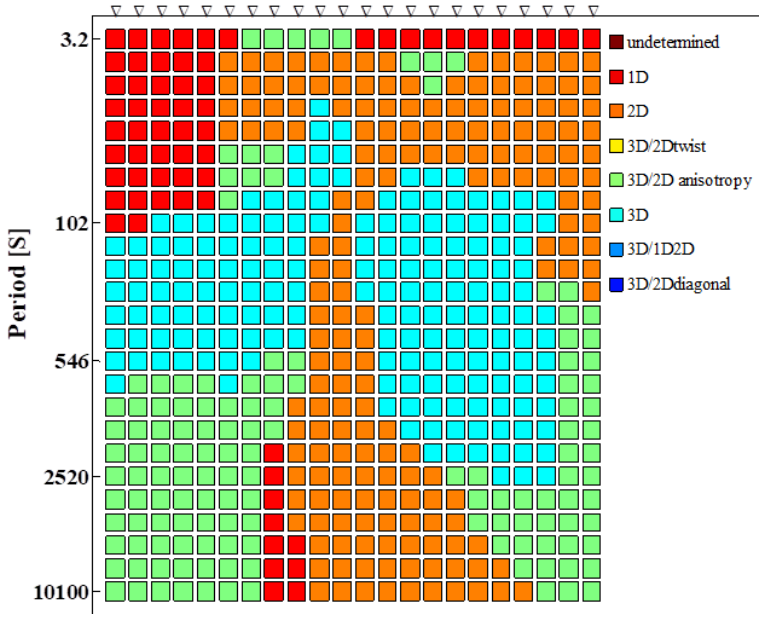

Fig 3. Dimensionality pattern corresponding to the responses of model 1a. All sites whose responses have been computed are shown.

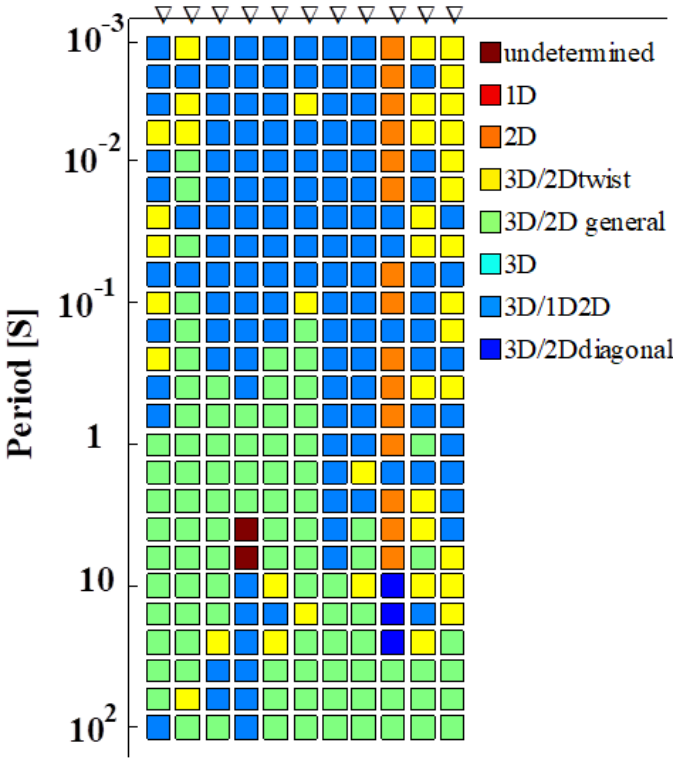

Figure 4. Dimensionality pattern corresponding to the responses of model 1b. All sites whose responses have been computed are shown.

However, precise interpretation of MT data requires distortion removal and recovering regional impedances.

Although WAL rotational invariants could recognize correctly the dimensionality and distortion effects inherent in the synthetic data, but they cannot remove distortions and retrieve regional impedances. The GB distortion decomposition approach was applied for the synthetic data set. The recovered and undistorted regional responses are exemplary shown for the site l04 (Fig. 5). It appears that the proposed approach recovered each of the regional responses, accurately.

To summarize, the subsequent use of WAL invariants and the GB method could successfully classify distortion types and recover the properties of regional 2D structure.

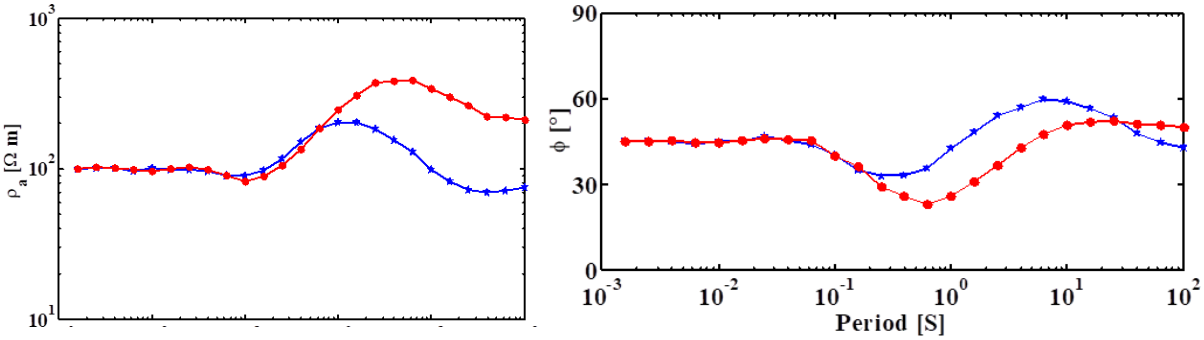

Fig 5. The recovered regional MT responses (symbols) are compared to the true theoretical ones (solid lines) for station l04 in the second synthetic example.

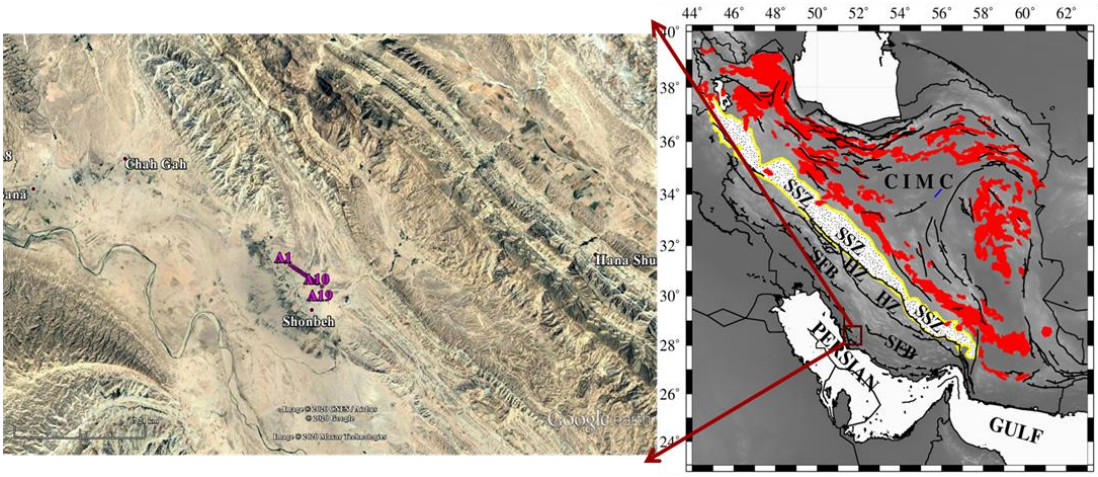

Fig 6. Geological map showing the location of MT sites. Also shown are the main structural units (Simply Folded Belt (SFB), High Zagros (HZ), Sanandaj-Sirjan Zone (SSZ), Central Iranian Micro Continent (CIMC)) and the major faults.

3 Application to the field data

A field dataset from southwest Zagros, recorded at 19 stations in a period range of [10^{-4}, 0.4] second was considered. To assess the inherent complexity of the MT data, dimensionality, strike and distortion analyses were carried out by the proposed two-stage procedure.

3-1 Geological setting

The geodynamic framework of the Zagros region is composed of the two Arabia and Eurasia plates moving westerly relative to the mantle. Eurasia is faster and overrides the Arabia SW ward, up to 16-25 mm/yr, leading to the formation of NW-SE trending Zagros mountain range because of the continent-continent collision. The High Zagros fault separates the Zagros fold and thrust belt (ZFTB) into the Zagros Simply Folded Belt (SFB) in the southwest and the High Zagros (HZ) in the northeast. The SFB which has lower topography than HZ and is more active accommodates the most present-day deformation of the range (Elliot et al., 2015). A 10-14 km-thick sedimentary cover is deposited on the Arabian passive margin throughout the most Phanerozoic times and is detached from underlying crystalline basement by late pre-Cambrian to Cambrian Hormuz formation evaporates (Sherkati et al., 2006). A thick basal evaporite (Hormoz salt) is overlain by the Paleozoic to early-Miocene series composed of Carbonate and clastic units with minor evaporative levels. Our MT profile is located within the thick, folded sedimentary cover of the south eastern SFB (see Fig. 6).

3-2 Bahr and WAL rotational invariants

Fig. 7 represents Bahr invariants for the station A08. While the calculated μ remains above 0.1, η is below 0.3, suggesting that the regional structure is 2D rather than 3D or 1D. Class 5 is the appropriate category for the data. This reasoning is independently confirmed by the GB decomposition results that will be discussed in the next section.

Rotational invariants used in Bahr's classification for all sites and all periods are presented in Fig. 8. The Swift skew values exceed the threshold of 0.1 at most periods, representing galvanic distortions contaminated measured data (Fig. 8a). Since at several sites, the regional 1D indicator (μ) is above the threshold proposed by Bahr (1991) and the 3D/2D skew (η) is lower than the corresponding threshold, the regional resistivity structure generating our data is most likely of 2D.

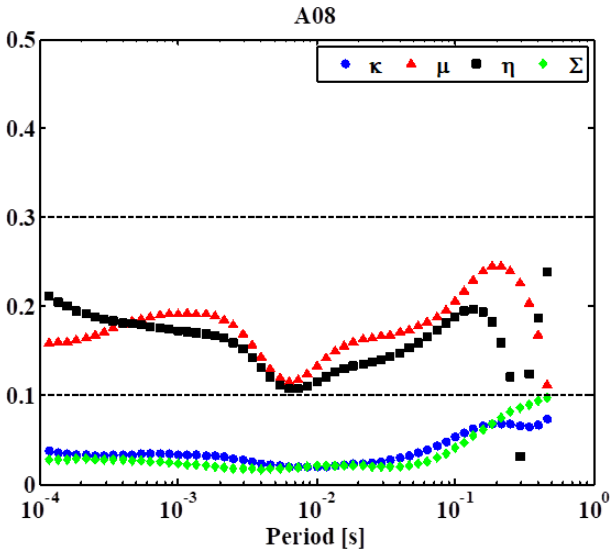

Fig 7. Bahr rotational invariants at the station A08. Regional 1D indicator, μ, is above the threshold value through the whole period range.

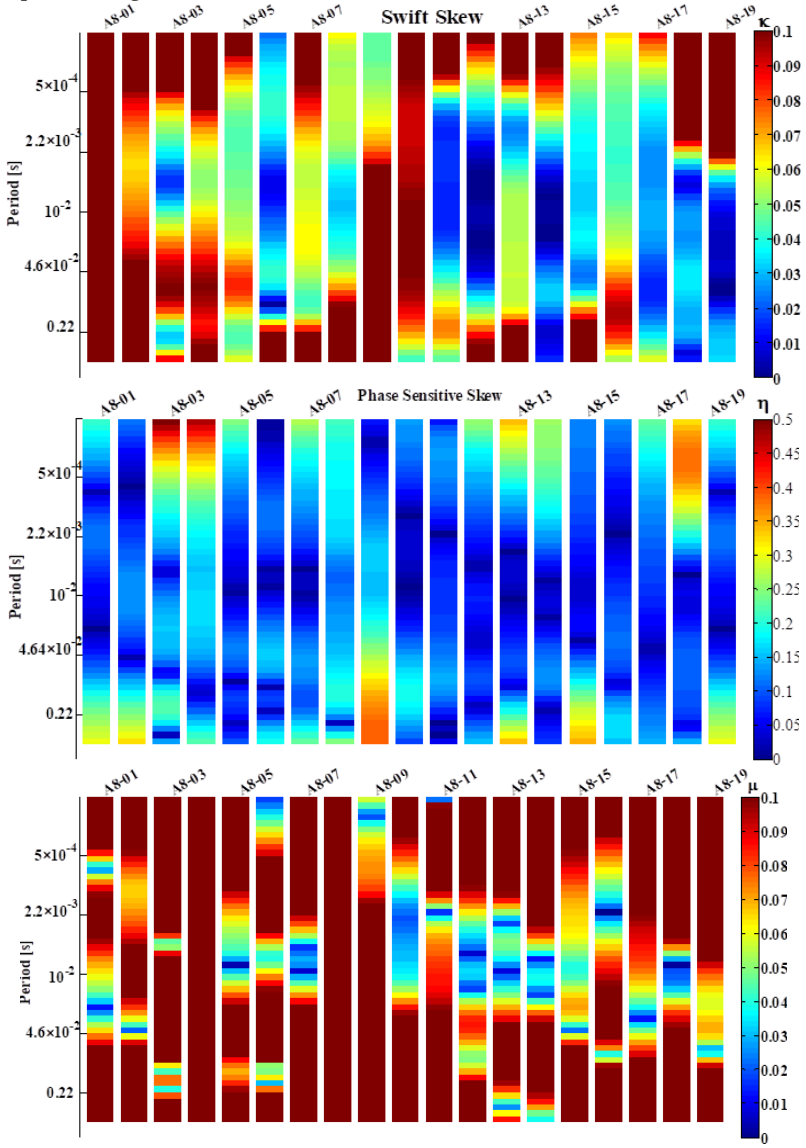

Fig 8. (a) Swift skew (b) 1-D regional indicator (c) phase sensitive skew calculated for all sites at all periods.

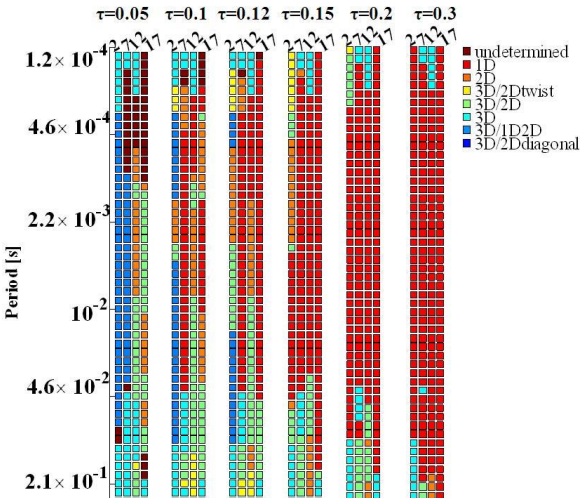

Fig 9. The results of dimensionality analysis of MT data set at sites a02, a07, a12, a17, considering different threshold values: 0.05, 0.1, 0.12, 0.15, 0.2, 0.3.

Different threshold values (0.05, 0.1, 0.12, 0.15, 0.2 and 0.3) for the WAL invariants were tested to determine dimensionality for a subset of AMT data set. The dimensionality results associated with four representative sites are presented in Fig. 9.

It is a subjective decision to choose the optimum threshold value for the invariants. An extreme threshold value of τ = 0.05 results in an inconsistent dimensionality pattern. Increasing threshold values resulted in a decreasing number of undetermined dimensionality cases and a more uniform dimensionality pattern (Fig. 9). However, it should be noted that a higher threshold value is a consequence of a higher data error assumption (Marti et al., 2009). Our numerical studies show that intermediate threshold values of 0.12, 0.15, and 0.2 for I1, I2, ... , I7 invariants, and the threshold value of 0.1 for Q invariant provide a stable and consistent dimensionality pattern.

Dimensionality pattern at different periods of all sites is presented in Fig. 10. The results confirm 1D or 2D regional geo-electric structure with many periods exhibiting either 1D or 2D responses and some rare 3D/2D and 3D responses at longer periods.

3-3 Galvanic-distortion identification and removal

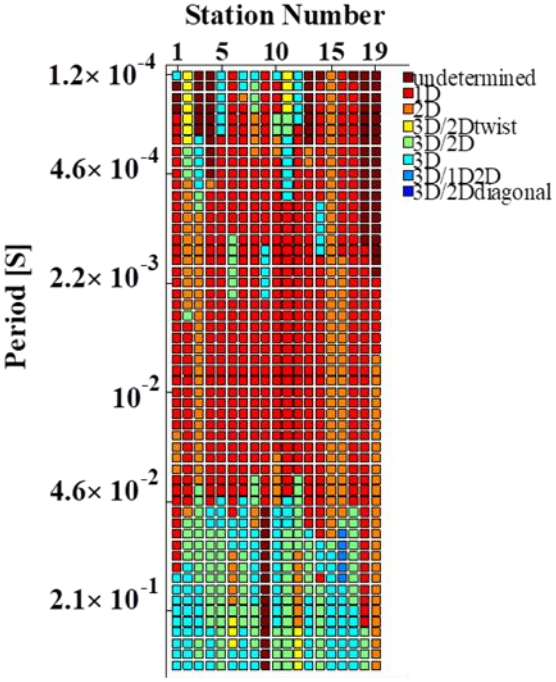

Fig 10. Dimensionality pattern obtained from WAL rotational invariants for all periods at each measurement site.

In this study, the GB method was applied to determine galvanic distortion effects and remove them from measured impedances. The results of distortion decomposition, presented in this paper, were based on an impedance error floor of 1% which corresponds to 2% and 0.6˚ error floors

for the apparent resistivities and phases.

Fig. 11 shows the results for six representative sites. Distortion parameters (i.e., shear and twist angles) whose tangents determine different elements of **S** and **T** matrices in equation (3) as well as the phase difference of the principal regional impedances, are presented in these figures. The decomposition parameters for joint inversion of three periods and one-period decade are illustrated in the first and second rows of diagrams for each site (Fig. 11).

Twist and shear angles reveal an approximately period-independent behavior throughout the entire period range and are between [-10˚, 10˚]. At periods less than 0.01 second, the phase differences of regional impedances are almost zero, indicating a 1D regional geoelectric structure.

The root mean square of the GB model measures the goodness of fit between the decomposition model and the observed data and provides an estimate of three dimensionalities of the subsurface regional structure (Adetunji et al., 2015). Fig. 12 shows the shear and twist angles and the RMS misfit at each period.

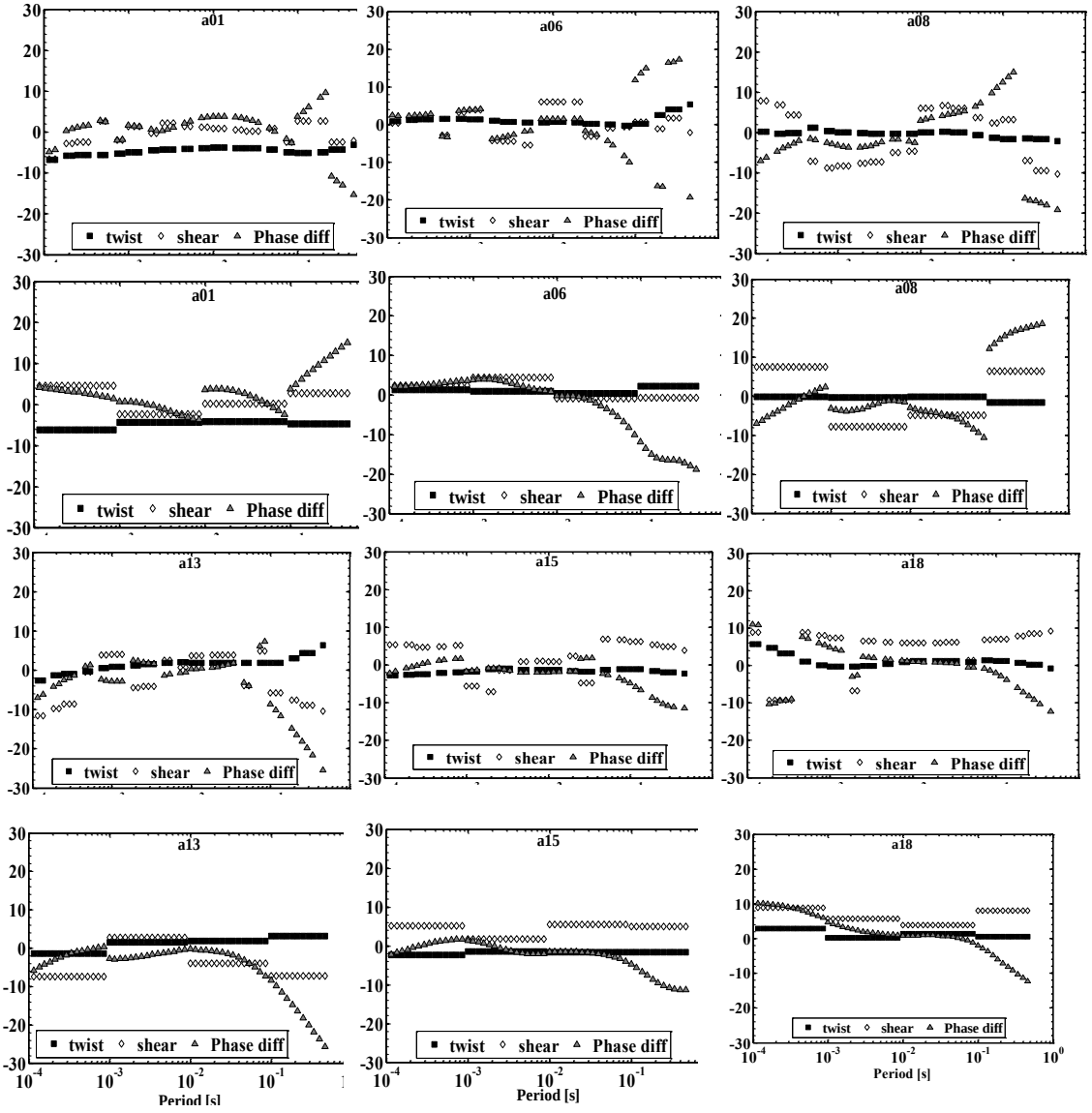

Fig 11. Frequency independent distortion parameters calculated at six representative sites.

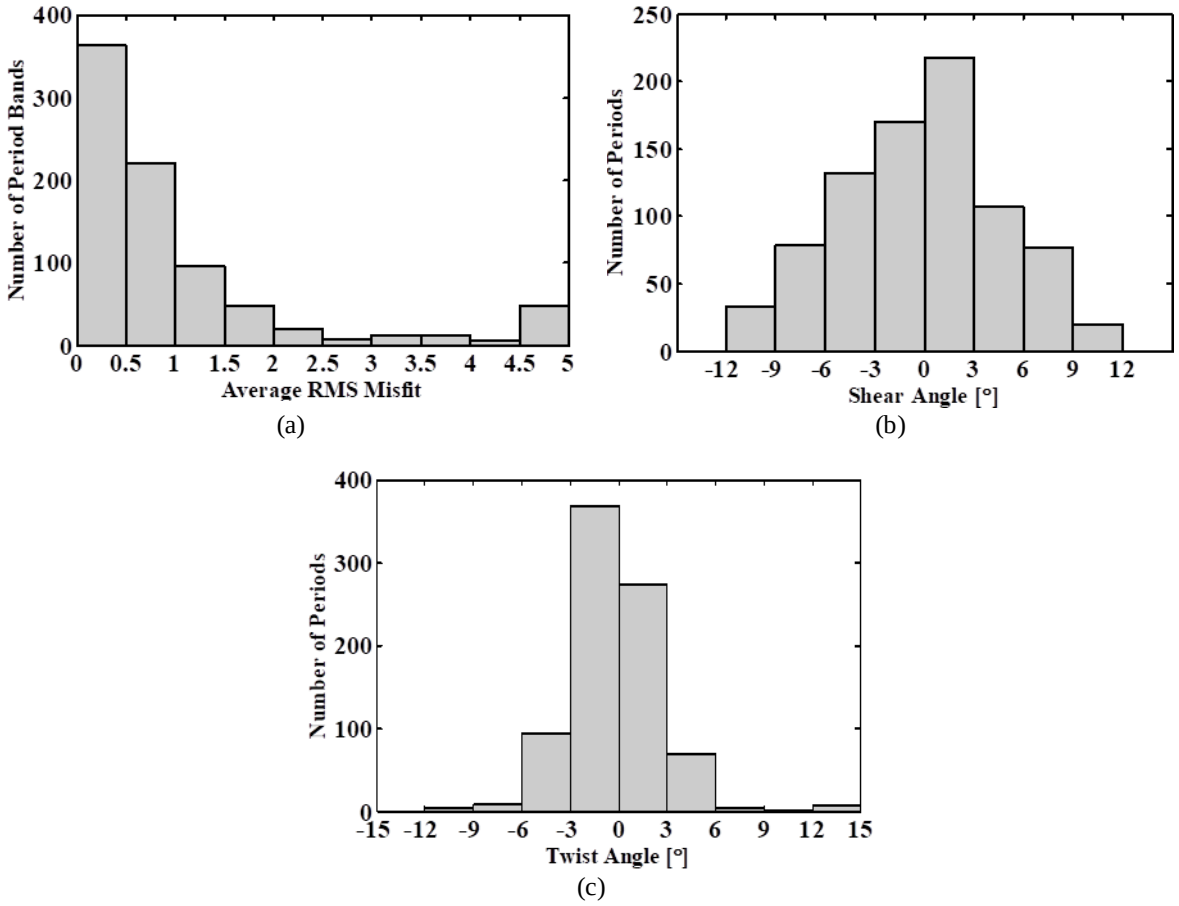

Fig 12. Distribution of the twist and shear angles and the average RMS misfits.

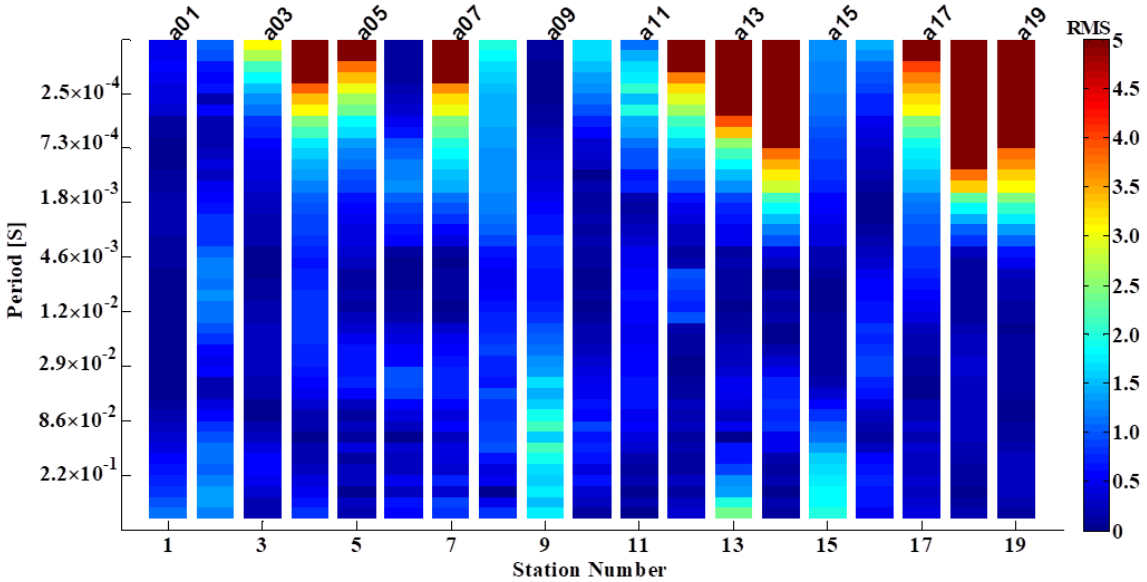

Fig 13. Data RMS misfits from unconstrained GB decomposition model for each site along MT profile over the whole period range.

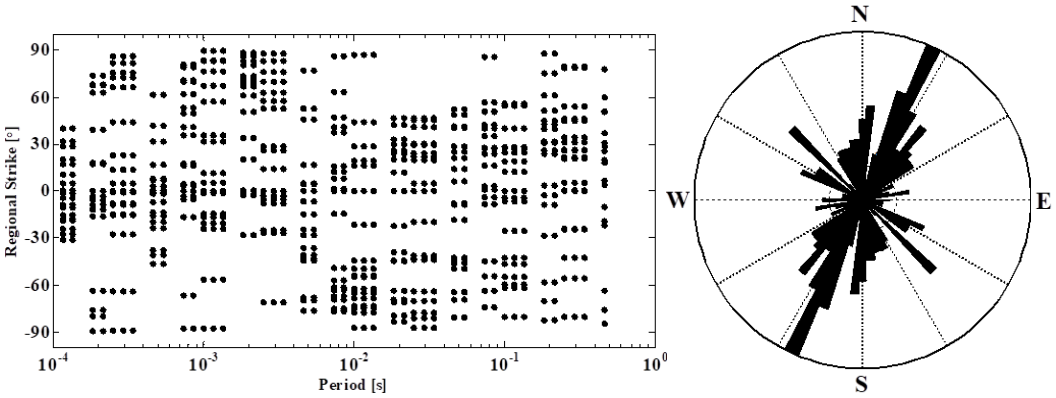

(a) (b)

Fig 14. (a) Regional strike direction as a function of period for all sites of the A8 profile, estimated from an unconstrained GB analysis. (b) Rose diagram of the regional geo-electric strike angle at periods where split in the principal phases are greater than 5˚.

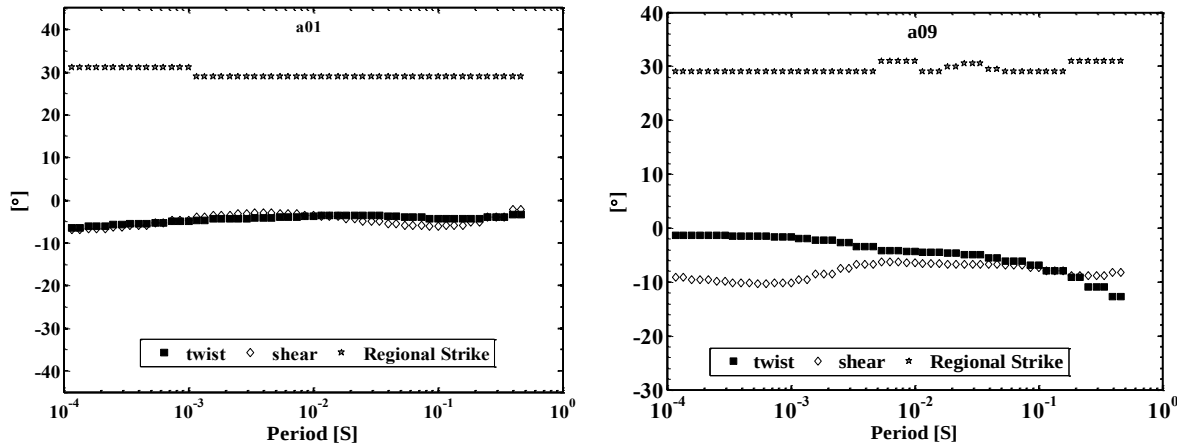

Fig 15. Shear and twist angles from GB analysis with strike angle fixed at 30˚.

The results indicate a moderate to low level of distortions in the studied area. The distribution of the RMS misfits shows an average misfit of less than 1 for most of the periods, which is an acceptable value. High values of the RMS occur in the shortest periods (Fig. 13), which could be explained by the predominantly 1D regional structure at these periods, as recovered by the impedance invariants (Fig. 8b).

The strike angles from unconstrained GB decomposition, when plotted as a function of period, do not show a preferred azimuth direction (Fig. 14a). The periods were removed where the data are 1D. Fig. 14b shows a rose diagram of strike angles at periods where the split in principal phases is greater than 5˚. The dominant strike azimuth of the regional geo-electric structure is about N30˚E.

The two regional impedances were derived by removing distortion effects from measured data. The geo-electric strike azimuth and the distortion parameters, which are frequency independent according to the GB model, were constrained sequentially. First, the regional strike was fixed to 30˚ which yields stable estimates of the twist and shear angles with period (e.g., Fig. 15 shows the results for the stations 1 and 9). Finally, the regional impedances were estimated by constraining regional strike, twist and shear angles to 30˚, -5˚and -5˚, respectively. Regional impedances obtained from GB decomposition together with the measured sounding curves are presented in Fig. 16. Galvanic distortion effects, mixing the Z_{xy} and Z_{yx} in the apparent resistivity curves, are evident in the measured soundings.

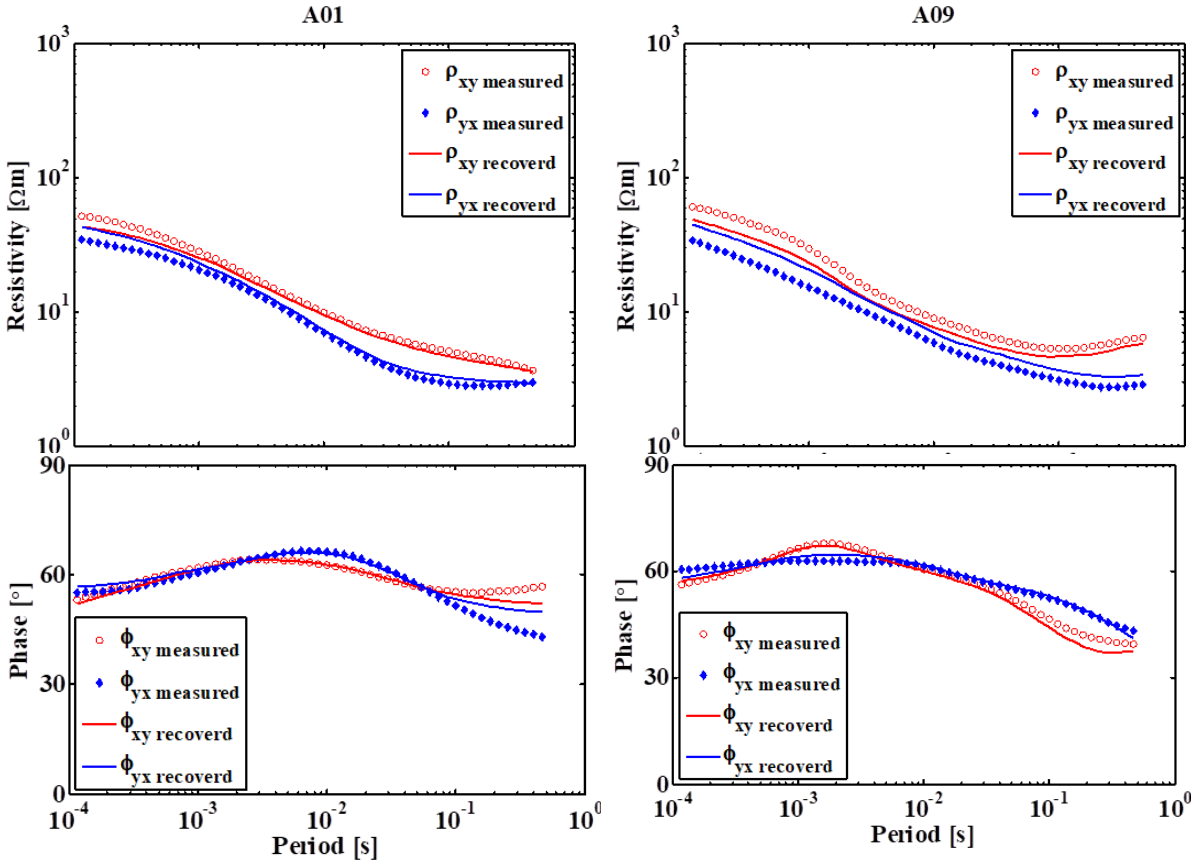

Fig 16. Measured apparent resistivity and phase curves (symbols) and the recovered regional responses recovered by the GB method (solid lines) for sites A01 and A09.

4 Conclusion

Two basically different approaches (the GB method and the WAL invariants) for dimensionality and distortion analysis were constrained sequentially with numerical experiments involved real and synthetic datasets.

Two synthetic datasets are examined to demonstrate the limitations of the individual methods. It is displayed that in electrically anisotropic situations, the GB method produces artifacts leading to non-existent structures, responsible for distortion effects. Although the WAL invariants provide a practical tool to obtain information about the dimensionality of complex regional structure, but they could not correct data and recover the regional responses. The results suggest that the combination of both methods yields more comprehensive consequences than those of the individual implementations of the WAL invariants and the GB method.

The proposed two-stage procedure of MT data analysis was applied for a field dataset acquired in the southwest of Iran. At the first step, the application of rotational invariants showed that there is no sign of electrical anisotropy in dimensionality pattern and the regional conductivity structure can be considered predominantly as 2D with some superimposed distortions from local 3D conductivities. Next, the GB method was applied to determine and remove distortion effects and to obtain superior estimates of regional MT parameters (strike direction and impedances). The method suggested a global strike direction of N30°E for regional conductivity structure and recovered corresponding impedances, successfully.

Acknowledgements

The authors express their gratitude to Iran Office of Vice-presidency for Science and Technology, office of drought, erosion and environmental affairs for kindly providing the field data used in this work

References

Adetunji, A. Q., Ferguson, I. J., and Jones, A. G., 2015, Re-examination of magnetotelluric responses and electrical anisotropy of the lithospheric mantle in the Grenville Province, Canada: J. Geophys. Res., **120**, doi 10.1002/2014JB011713.

Bahr, K., 1991, Geological noise in magnetotelluric data: a classification of distortion types: Physics of the Earth and Planetary Interiors, **66**, 24–38.

Brasse, H**.,** and Rath, V., 1997, Audiomagnetotelluric investigations of shallow sedimentary basins in northern Sudan: Geophys. J. Int., **128**(2), 301–314.

Caldwell**,** T. G., Bibby, H. M., and Brown, C., 2004, Themagnetotelluric phase tensor: Geophys. J. I., **158**(2), 457–469.

Cerv, V., Pek, J., and Menvielle, M.,2010, Bayesian approach to magnetotelluric tensor decomposition: Annals of Geophysics, **53**(2), 21–32.

Chave, A. D., and Jones, A. G., 2012, TheMagnetotelluric Method – Theory and Practice: Cambridge University Press, Cambridge, 570 p.

Elliott, J. R., Bergman, E. A, Copley, A. C., Ghods, A. R., Nissen, E. K., Oveisi, B., Tatar, M., Walters, R. J., Yamini-Fard, F., 2015, The 2013 Mw 6.2 Khaki-Shonbe (Iran) earthquake: insights into seismic and aseismic shortening of the Zagros sedimentary cover: Earth and Space Science, **2**, 435–471, doi 10.1002/2015EA000098.

Giroux, B., Chouteau, M., Descloitres, M., and Ritz, M., 1997, Use of the magnetotelluric method in the study of the deep Maestichtian aquifer in Senegal: Journal of Applied Geophysics, **38**, 77-96.

Groom, R. W., and Bailey, R. C., 1991, Analytical investigations of the effects of near surface three-dimensional galvanic scatterers on MT tensor decomposition: Geophysics, **56**, 496–518.

Heise, W., and Pous, J.,2001, Effects of anisotropy on the two-dimensional inversion procedure: Geophys. J. I., **147**(3), 610-621, doi 10.1046/j.0956-540x.2001.01560.x.

Ledo, J., 2006, 2-D versus 3-D magnetotelluric data interpretation: Geophysics, **27**, 511–543.

Mahallati, A., and Montahaei, M., 2019,Application of MT forward modeling responses for time-lapse monitoring of the subsurface electrical resistivity changes: Journal of the Earth and Space Physics, **46**(4), 1-12, doi:10.22059/JESPHYS.2019.279194. 1007107**.**

Martí, A., Queralt, P., and Ledo, J., 2009, WALDIM: a code for the dimensionality analysis of magnetotelluric data using the rotational invariants of the magnetotelluric tensor: Computers & Geosciences, **35**(12), 2295–2303.

Martı´, A.**,**Queralt, P., Ledo, J., and Farquharson, C., 2010, Dimensionality imprint of electrical anisotropy in magnetotelluric responses: Physics of the Earth and Planetary Interiors, **182**, 139–151, doi:10.1016/j.pepi.2010.07.007.

McNeice, G. W., and Jones, A. G., 2001, Multisite, multifrequency tensor decomposition of magnetotelluric data: Geophysics, **66**(1), 158–173.

Pek, J., and Verner, T., 1997, Finite difference modelling of magnetotelluric fields in 2-D anisotropic media: Geophysical Journal International, **128**, 505–521.

Rodi, W., and Mackie R. L., 2001, Nonlinear conjugate gradients algorithm for 2-D magnetotelluric inversion:

Geophysics,**66**(1), 174–187.

Sherkati, S., Letouzey, J., and Frizon de Lamotte, D., 2006, Central Zagros fold-thrust belt (Iran): New insights from seismic data, field observation, and sandbox modeling: Tectonics, **25**, TC4007, doi:10.1029/2004TC001766.

Tarabees, B., Tewksbury, C., Mehrtens, J., and Younis, A., 2017, Audio-magnetotelluric surveys to constrain the origin of a network of narrow syn-clines in Eocene limestone, Western Desert, Egypt: Journal of African Earth Sciences, **136**, 168–175.

Weaver, J. T., Agarwal, A. K., and Lil-ley, F. E. M., 2000, Characterization of the magnetotelluric tensor in terms of its invariants: Geophys. J. I., **141**(2), 321–336.

Zhang, P., Roberts, R. G., and Pederson, L. B., 1987, Magnetotelluric strike rules: Geophysics, **52**(3), 267–278.